



OPEN

## Anchoring effect of NPR cables under dynamic conditions and its engineering applications

Jie Hu<sup>1,2</sup>, Manchao He<sup>1</sup>, Zhigang Tao<sup>1</sup> & Haijiang Zhang<sup>2,3</sup>✉

Anchor cable failures due to dynamic loads are common in rock engineering. Traditional cables could be invalid to accommodate large displacement and deformation in geomaterials. Cable body failure often occurs due to limitations in mechanical characteristics and small deformation of traditional anchor cables. The new Negative Poisson's ratio (NPR) cable has the mechanical properties of high strength, toughness, and impact resistance due to its special structure. This study investigated the response of NPR cable anchorage systems under dynamic loading through laboratory tests and numerical modeling. The dynamic pull-out tests on NPR cable under drop hammer loading were conducted to examine the behavior of dynamic perturbation mitigation. To investigate the intricate NPR cable-rock interaction, a coupled model utilizing the distinct element method (DEM) and the finite difference method (FDM) was established. The NPR cable was encircled by grouted concrete and sandstone modeled with discretized particles using the distinct element method. The numerical results and the NPR cable-rock interaction under dynamic loading were carefully analyzed and discussed. The NPR cable-rock interaction, including the relative sliding displacement between the cone and the pipe, the accumulated relative sliding displacement between the cone and the pipe, the radial displacement of the pipe, and the contact forces of concrete and rock, were carefully studied through numerical simulation. Furthermore, a microscopic analysis was conducted to investigate the failure modes exhibited by the grouting material and the surrounding rock. Finally, NPR cables are utilized to reinforce the slope stability in open-pit mines. Their applications demonstrate that NPR cables can mitigate slope failures and play a crucial role in anticipating and providing timely warnings of slope instability, alongside a comprehensive slope stability monitoring system. This study offers valuable insights that can contribute to predicting and enhancing the performance of NPR cables in mitigating the effects of dynamic disasters.

**Keywords** Energy-absorbing cable, Drop hammer loading, DEM-FDM coupled method, Cable-rock interaction, Field application

Anchor cable is an effective and widely applied supporting technique in geotechnical engineering<sup>1,2</sup>. In rock engineering, rock cables are commonly employed as a means to ensure the stability and integrity of geo-bodies<sup>3-5</sup>. They can be categorized into strength, ductile, and energy-absorbing cables according to the classification of Li<sup>6</sup>. Strength and ductile cables provide a high load-bearing capacity or good ductility, while energy-absorbing cables possess exceptional strength and remarkable deformation capacity, making them ideal support equipment. Various energy-absorbing bolts have been developed, such as the Cone bolt<sup>7</sup>, the Garford Dynamic Solid Bolt<sup>8</sup>, Roofex Bolt<sup>9</sup>, and the D-bolt<sup>10</sup> J-bolt<sup>11</sup>. Furthermore, an innovative energy-absorbing cable/bolt with both constant resistance and large deformation capabilities, featuring a unique negative Poisson's ratio (NPR cable/bolt)<sup>12</sup> has been designed, and a large number of indoor experimental tests<sup>13,14</sup> and in situ tests<sup>15</sup> have been performed on NPR cables/bolts, concluding that they can maintain almost constant resistance during elongation<sup>16-18</sup>.

Rock cables typically endure three primary loading types: axial loading, shear loading, and a combination of both<sup>19</sup>. The axial loading of rock cables can be done statically and dynamically using the axial pull-out testing method both in-situ and in the laboratory<sup>20-23</sup>. Static shear loading can be achieved either through the single shear method or the double shear technique, depending on the availability of multiple joint faces for

<sup>1</sup>State Key Laboratory for Tunnel Engineering, China University of Mining and Technology (Beijing), Beijing 100083, China. <sup>2</sup>Collaborative Innovation Center for Prevention and Control of Mountain Geological Hazards of Zhejiang Province, Shaoxing University, Shaoxing 312000, China. <sup>3</sup>Key Laboratory of Rock Mechanics and Geohazards of Zhejiang Province, Shaoxing University, Shaoxing 312000, China. ✉email: haijiang1086@usx.edu.cn

shear testing<sup>24–26</sup>. Furthermore, it is of utmost significance to assess the efficacy of rock cables performance when subjected to dynamic loads, particularly during seismic events, explosive activities, and rock burst<sup>19,27</sup>. Drop hammer test<sup>23,28–30</sup> and the modified Split Hopkinson Pressure Bar (SHPB) test<sup>16</sup>, as a dynamic testing technology, have been widely utilized for evaluating the performance of supports.

However, the NPR cable–rock interaction exhibits significant differences compared to that of traditional cables. As a support system widely used in slope reinforcement<sup>16,31–33</sup> and underground engineering<sup>12,34</sup>. The sleeve pipe of the NPR cable is encapsulated within the grouting material, resulting in its confinement within a borehole drilled into the rock mass. During the intrusion of the cone into the sleeve pipe, resulting in its tubular expansion, the cable's surrounding environment experiences both shearing forces and substantial normal compression, along with circumferential extension. These combined effects have the potential to affect the development and evolution of the pull-out strength. Hence, its behavior under confining pressure and its interaction with the rock mass warrant careful investigation.

In describing the mechanical behavior of a cable reinforcement system, it is crucial to consider two distinct deformational characteristics: firstly, the brittle nature of the rock and grouting material, which exhibits discrete deformations during failure, such as crack rupturing, opening, and closing; secondly, the ductile nature of the cable body or its components, which undergoes continuous deformation under normal operating conditions<sup>35,36</sup>. The concurrent presence of these deformational characteristics strongly suggests the necessity of a suitable tool capable of interpreting both aspects in any endeavor to simulate the cable reinforcement system. The integration of the discrete-element method (DEM) and finite-difference method (FDM) emerges as a potentially promising strategy, wherein FDM handles the behavior of the cable, while DEM simulates the dynamics of the surrounding bodies<sup>37,38</sup>. Dong et al.<sup>39</sup> introduced an innovative FEM/DEM coupled numerical method for analyzing the pull-out failure of corroded rock bolts. He et al.<sup>40</sup> examined the dynamic response of the NPR anchor cable supporting the roadway under explosion conditions, employing a combined approach of the finite element method and the discrete element method. Li et al.<sup>35</sup> employed a coupled FEM/DEM numerical method to examine the characteristics of the CRLD cable–rock interaction under static pull-out loading conditions.

The occurrence of landslides on an engineering scale is a typical dynamical phenomenon, which undergoes a transition from steady-state static deformations to dynamic slip or catastrophe, which is macroscopically realised as a sudden change in displacement and stress drop. The stability of slopes is often reinforced by anchor cables. While landslides are typical dynamic processes, the mechanical performance of anchor cables under dynamic conditions therefore plays a crucial role in mitigating landslide hazards. In view of the high strength and toughness exhibited by NPR cables under static loading conditions<sup>12–18</sup>, the present study was carried out to investigate their applicability in dynamic disaster control. In this paper, the response of NPR cables under dynamic loading is explored through drop hammer tests, and its mechanism of NPR cable–rock interaction under dynamic conditions is elucidated through a coupled DEM-FDM numerical approach, providing insights that help predict and refine the efficiency of NPR cables in mitigating dynamic hazards. Finally, a specific slope case is used to illustrate the effectiveness of NPR cables for reinforcement and early warning. The subsequent sections of this paper are structured as follows. In “[Experimental results and numerical model](#)” section, drop hammer tests of NPR cables under dynamic loading are presented and the FDM model of the cables is validated. In “[DEM-FDM coupled model and its calibration](#)” section, the extended coupled DEM-FDM model and its validation are described in detail. In “[Numerical results and discussions about the NPR cable–rock interaction](#)” section, the DEM-FDM numerical results are presented and an in-depth discussion of the NPR cable–rock interaction mechanism under dynamic loading is presented. In “[Field application](#)” section, an open pit mine uses NPR cables to improve slope stability, effectively predicting and issuing early warnings of potential slope tries. In “[Conclusion](#)” section provides the conclusions of this study.

## Experimental results and numerical model

### Drop-hammer impact experiments of the NPR cable

The drop impact test system comprises a steel frame with a vertical height of 7200 mm, an automatic sample delivery system, a hydraulic clamping device, a tension device providing a maximum impact height of 4000 mm, a drop hammer with a gravity of 53 kN, a hydraulic buffer system, and a control console, as depicted in Fig. 1. NPR cables exhibit a significant and consistent resistance while enduring substantial deformation, and the corresponding structure is shown in Fig. 2a. The components of the NPR cable are shown in Fig. 2b. A comprehensive list of the mechanical and geometric parameters is provided in Table 1.

For dynamic pull-out tests under drop-hammer impact loading, the NPR cable was installed vertically through the center hole of the hammer, and one end of the pipe was securely fastened to the test system's top using appropriate holding equipment, as given in Fig. 3a. The hammer was uplifted to an impact height of 0.4 m using the takeup equipment tension device in Fig. 3b, and then dropped until it impacted the plate bottom to transfer the dynamic loads to the attached strands, as shown in Fig. 3c,d. It is noteworthy that lubricant oil was applied to the interface between the cone and pipe during the test to facilitate smooth sliding; the hammer impact height was counted from the plate but not the system bottom to ensure the same dynamic loads during dropping.

The dynamic pull-out tests were performed on identical NPR cable samples. According to Fig. 4a, taking the ideal result after 33 impacts as an example, the cones are extruded from the pipe. the relative sliding displacement between the cone and the pipe can be divided into four stages. The relative sliding displacement per impact increases sharply since the small-end diameter of the cone body is slightly smaller than the inner diameter of the pipe. Then, it decreases slowly when the tubular expansion occurs until it reaches a constant residual value (approximately 37 mm). The friction effect causes wear on the cone body, increasing the sliding displacement under the single impact loading (approximately 60 mm). With the increasing wear, the cone body is quickly hauled out of the pipe. According to Fig. 4b, the resistances against the dynamic impacts can be estimated as 420



**Fig. 1.** Dynamic pull-out test system with drop hammer.

kN and 320 kN, and the reduced cone-pipe contact area can lower the resistance when the cone intrudes into and extrudes from the pipe.

#### FLAC3D model of the dynamic pull-out tests for NPR cable

For large-scale laboratory tests, examining every contributing factor by repeating experiments and ensuring reasonable results are not feasible. Due to these considerations, numerical simulations were employed to gain insights and propose significant improvements to these models, which are presented here. FLAC<sup>3D</sup> software was utilized to simulate the NPR cable. Static pull-out tests were modeled, and the numerical outcomes were cross-checked with experimental measurements to validate the physical parameters of the numerical model. Then, the drop hammer loads were estimated, and the dynamic pull-out tests were simulated. The numerical results of the simulated tests were validated in comparison to the experimental ones.

#### FLAC3D model of the NPR cable

The components of the NPR cable are presented in Fig. 5, and 11 points (A, B, C ... K) were selected to track the evolution of radial displacements induced by the cone-pipe relative sliding. The material properties of the NPR cable were assumed to be isotropic, while the cone and strand were modeled as elastic materials. Furthermore, to describe the pipe's perfect elastic-plastic behavior, the Mises yield criterion was implemented through the development and utilization of a corresponding dynamic link library (DLL). The interface attached to the pipe's inner surface enables relative sliding between the cone and the pipe. The normal and shear stiffness of this interface were determined based on recommendations from Itasca<sup>41,42</sup>, considering the elastic moduli of the pipe and cone, as well as the size of elements in proximity to the interface. The interface's behavior was then described using Coulomb sliding. As shown in Fig. 5, the end adjacent to the cone was constrained in the axial direction, while the distant end of the strand underwent a constant axial velocity of 20 mm/min until the cone was fully extruded from the pipe.

Table 2 lists the mechanical parameters of the NPR cable in the numerical simulation. Especially taking into account the mechanical and geometric parameters listed in Table 1, the friction angle of the interface was subjected to testing, as detailed in Table 2. More on the calibration of the parameters can be found in previous studies<sup>35</sup>. In the case of 8.5° friction angles, the constant resistance force sustained by the NPR cable was 500 kN, consistent with the static pull-out experimental results. In this case, the drawing force-axial displacement curve was numerically plotted during the static pull-out tests. A good agreement is observed after comparing it with the experimental results (Fig. 6). The drawing force rises linearly until it reaches 500 kN. It stays with the quasi-constant value throughout the cone-pipe relative sliding stage and quickly vanishes due to the disengagement between the pipe and cone. The above describes the constant resistance and large deformation phenomena. It is noteworthy that the axial displacement observed in the experimental results is shorter than the measured pipe length of 2000 mm. This discrepancy is attributed to the initial footing of the cone within the pipe during its installation. According to the above analysis, the parameters in Table 1 are validated for further investigation, considering the dynamic loading.

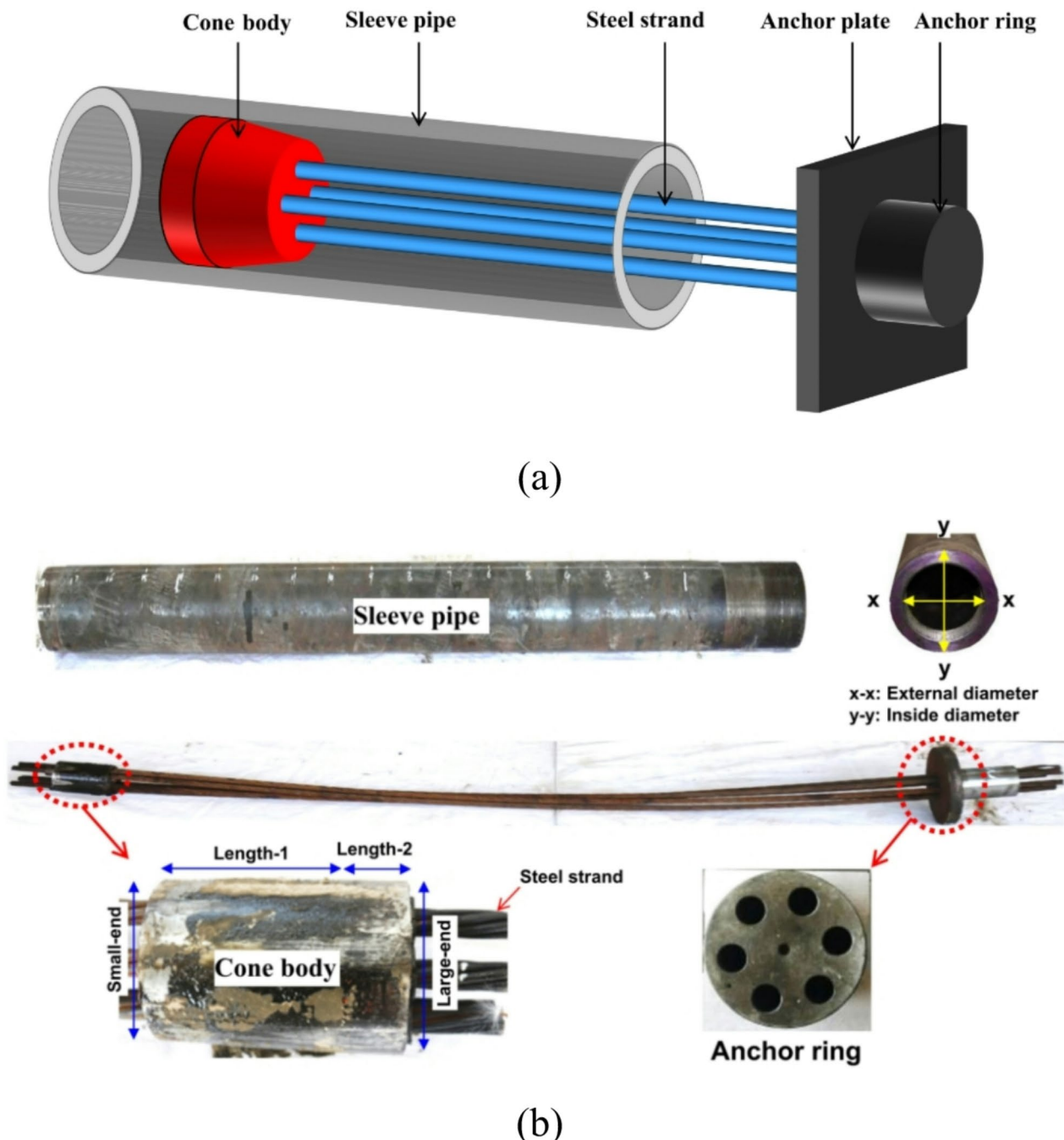


**Fig. 2.** (a) Structure scheme of the NPR cable, (b) component of the NPR cable.

Mechanical parameters		Geometric parameters (mm)									
$E$ (GPa)	206	Pipe			Cone body					Strand	
$\nu$	0.28	Outer diameter	Inner diameter	Length	Large-end diameter	Small-end diameter	Length-1	Length-2	Diameter	Length	
$\sigma_s$ (MPa)	730	121	87	2,000	93.5	83	85	25	22.4	2,800	

**Table 1.** Mechanical and geometric parameters of the NPR cable.

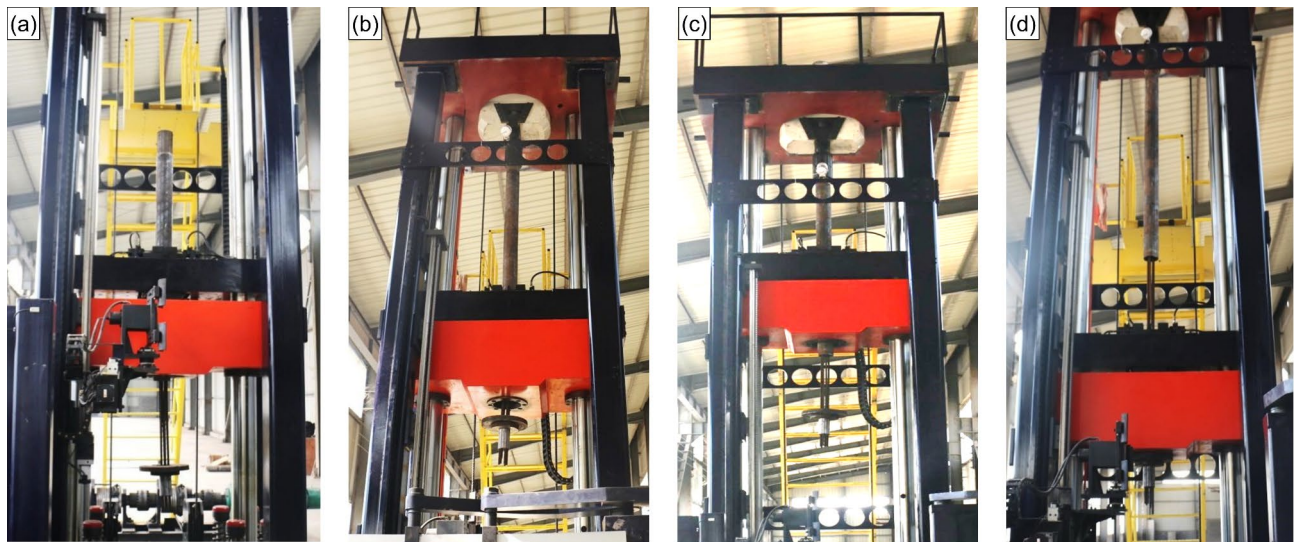


**Fig. 3.** Process of the dynamic pull-out test for the NPR cable. **(a)** Installation of the sample, **(b)** uplift of the hammer, **(c)** free fall of the hammer, **(d)** dynamic impact and elongation of the NPR cable.

#### *Numerical simulation of the dynamic pull-out tests*

Based on the above-mentioned numerical model, the dynamic loading induced by the drop hammer can be estimated using the following expression<sup>43,44</sup>:

$$A(t) = \begin{cases} \frac{1}{2}A_0 \left[ 1 - \cos\left(\frac{2\pi t}{\tau}\right) \right] & t_0 < t < \tau + t_0 \\ 0 & t < t_0, t > \tau + t_0 \end{cases} \quad (1)$$

where  $A_0$  represents the amplitude of the impulse,  $\tau$  denotes the impulse duration,  $f = l/\tau$  represents the frequency, and  $t_0$  the pulse starting time. Based on energy principles, in line with a dynamic loading corresponding to an impact height of 0.4 m, the parameters are determined as follows:  $A_0 = 7.61 \times 10^6$  kPa and  $f = 100$  Hz. Figure 7 illustrates the corresponding axial displacement histories tracked at the strand end during the first drop hammer impact loading. The axial displacement remains at about 23 mm after oscillations.

Based on the established NPR cable FDM numerical model, further numerical simulations of pull-out under dynamic conditions were carried out. According to Fig. 8a, after dynamic loading on the far end of the strand, the average cone-pipe relative sliding under one impact is about 22.5 mm, less than the reduced constant residual value (approximately 37 mm) at stage II in dynamic pull-out tests. The reasons can be divided into the following two aspects. On the one hand, although the lubricant oil was manually spread on the inner pipe wall to ensure relative sliding, this practice cannot guarantee absolute uniformity and moderation. On the other hand, the cone wears away due to the friction effect, and the contact area between the cone and the pipe undergoes a continuous reduction. This may be an important reason for the second plateau period as well as the final mutation of relative sliding displacement during the indoor test. Ideally, however, the relative sliding displacements should be close for each impact as long as the relative sliding displacements do not exceed the total length of the sleeve pipe, as shown by the numerical simulation results in Fig. 8a. After eliminating the disturbances from the factors of operators and materials, a consistent tendency between the dynamic pull-out tests under the drop hammer loading and its simulation is observed in Fig. 8a. Radial displacements at different pipe positions are shown in Fig. 8b. In drop hammer impact tests, 18 monitoring points (1–18) with an interval of 100 mm were set on the outer pipe surface, as presented in Fig. 8c. The deformation in both directions was obtained by measuring the x-x and y-y dimensions before and after the indoor experiment. The radial displacement was calculated in the numerical simulation by setting 11 monitoring points (A–K) on the outer pipe wall, as demonstrated in Fig. 8c. By comparing the test results in Fig. 8b, the radial displacement in the numerical test (approximately 2.7 mm) is slightly smaller than the lab test results of the first 11 dynamic loads due to the isotropic material property. In addition, the radial displacement in the laboratory test is discrete, arising from the reasons mentioned above and the anisotropic property of the pipe. Particularly following the 12th monitoring point, a substantial reduction in the radial displacement of the pipe is observed, attributed to the diminished contact area between the cone and the pipe.

The dynamic model of the NPR cable was validated. In the next Sections, the DEM-FDM coupled model will be presented, followed by the investigation into the NPR cable-rock interaction and the anchorage mechanisms.

#### **DEM-FDM coupled model and its calibration**

To investigate the interaction between NPR cables and rocks under dynamic conditions, a combined DEM-FDM approach was utilized, integrating the DEM code PFC<sup>3D</sup> 5.0 with the FDM code FLAC<sup>3D</sup> 6.0. The adoption of the explicit solution scheme and mixed discretization zoning enables FLAC<sup>3D</sup> to model continuum media

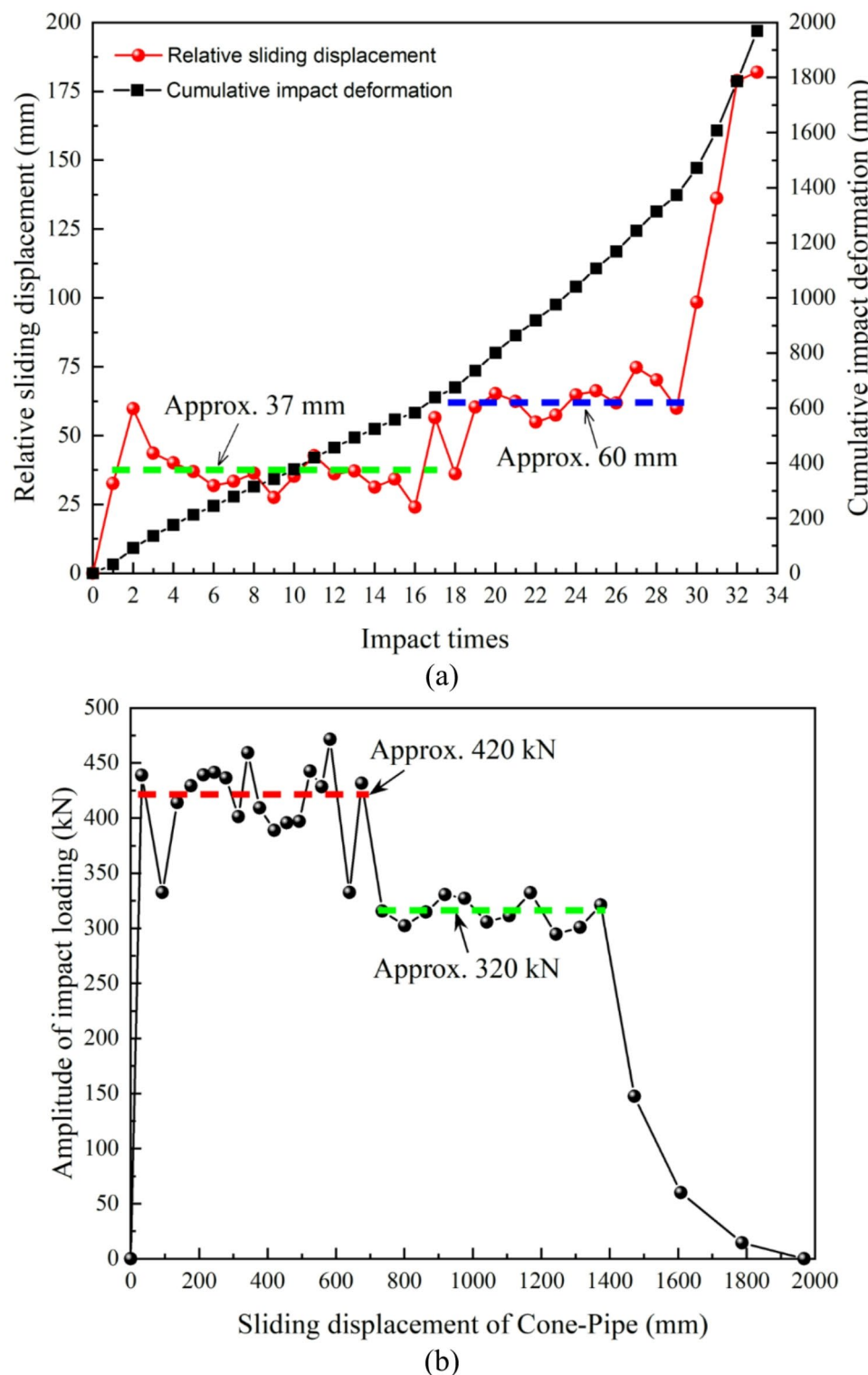


**Fig. 4.** Experimental results of the laboratory dynamic pull-out tests for the NPR cable. (a) Relative cone-pipe sliding against impact time under drop hammer loadings; (b) amplitude of dynamic loading against relative cone-pipe sliding curves.

using various constitutive models. In PFC<sup>3D</sup>, the currently adopted medium comprises spherical particles bonded together with a parallel bond model<sup>45,46</sup>. No meshing or constitutive models as employed in FLAC<sup>3D</sup> are required. The coupling scheme establishes an interface between the codes, facilitating the coordinated exchange of static and kinematic quantities within a unified physical time step. The induced pressures are relayed to PFC<sup>3D</sup> as boundary velocities. Subsequently, PFC<sup>3D</sup> undergoes its computational cycles and transmits the resulting

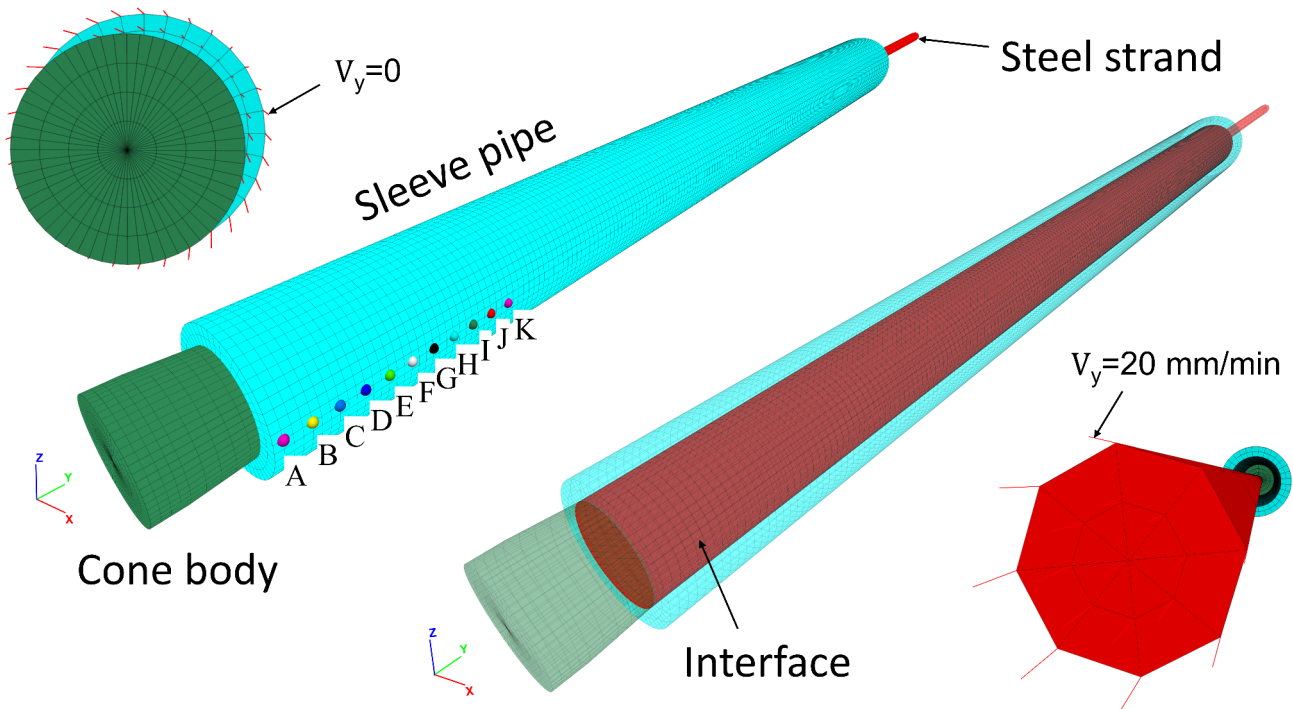


**Fig. 5.** Numerical model of the NPR cable: interface attached on the inner surface of the pipe and boundary conditions ( $v_y$  is the velocity in axial direction).

Elastic-plastic parameters	Yong's modulus (GPa)		Poisson's ratio		Tensile strength (MPa)	
	206	0.28	730			
Frictional angle (°)	27	17	12	9	8.5	7
Constant resistance force (kN)	1,200	860	620	540	500	420

**Table 2.** Mechanical parameters of the NPR cable.

boundary forces back to FLAC<sup>3D</sup>. This iterative process of transferring data back and forth between the codes continues until an equilibrium state is achieved<sup>37,47,48</sup>.

#### DEM-FDM coupled model

In the practical scenarios, the cable reinforcement system involves the cable, rock and anchorage agent in between<sup>39,49,50</sup>. A coupled DEM/FDM model was formulated to investigate the NPR cable-rock interaction, as depicted in Fig. 9a. The NPR cable was encircled by grouted concrete and sandstone, and their thicknesses are 14.5 mm and 136.74 mm, respectively. To achieve acceptable computational time, the concrete and surrounding rock near the cone were modeled by DEM (axial length of 300 mm) and FDM (axial length of 1700 mm), as illustrated in Fig. 9b.

The DEM part contains 185,492 particles exhibiting a uniform distribution, and their radii for the concrete and sandstone are 1.55–2.59 mm and 2.80–4.66 mm, respectively. The radial velocities of outer layer grid points of the FDM body were fixed, and a settled wall bonded the surface particles of the DEM body. The far end of the strand was subjected to dynamic loading according to Eq. (1).

#### Mechanical parameters and calibration in DEM

The initial step towards conducting a reliable numerical analysis involves identifying model parameters that facilitate the attainment of reasonably global behavior. The macro-mechanical parameters of sandstone were determined by the uniaxial compressive tests in the laboratory, and concrete C30 is listed in Table 3 from the Technical Code for Building Slope Engineering (GB 50330–2013) of China.

To calibrate and validate the micro-parameters of rock and concrete within the Discrete Element Method (DEM) framework, uniaxial compression and tension tests are conducted. The cylinder DEM model with a uniform radius distribution of particles was installed, with the same particle radii as the coupled DEM-FDM model of the NPR cable reinforcement system. In the uniaxial compression test, the top wall was loaded with an axial velocity of 0.004 mm/min (or –0.004 mm/min for the uniaxial tensile test), and the bottom one was frozen.

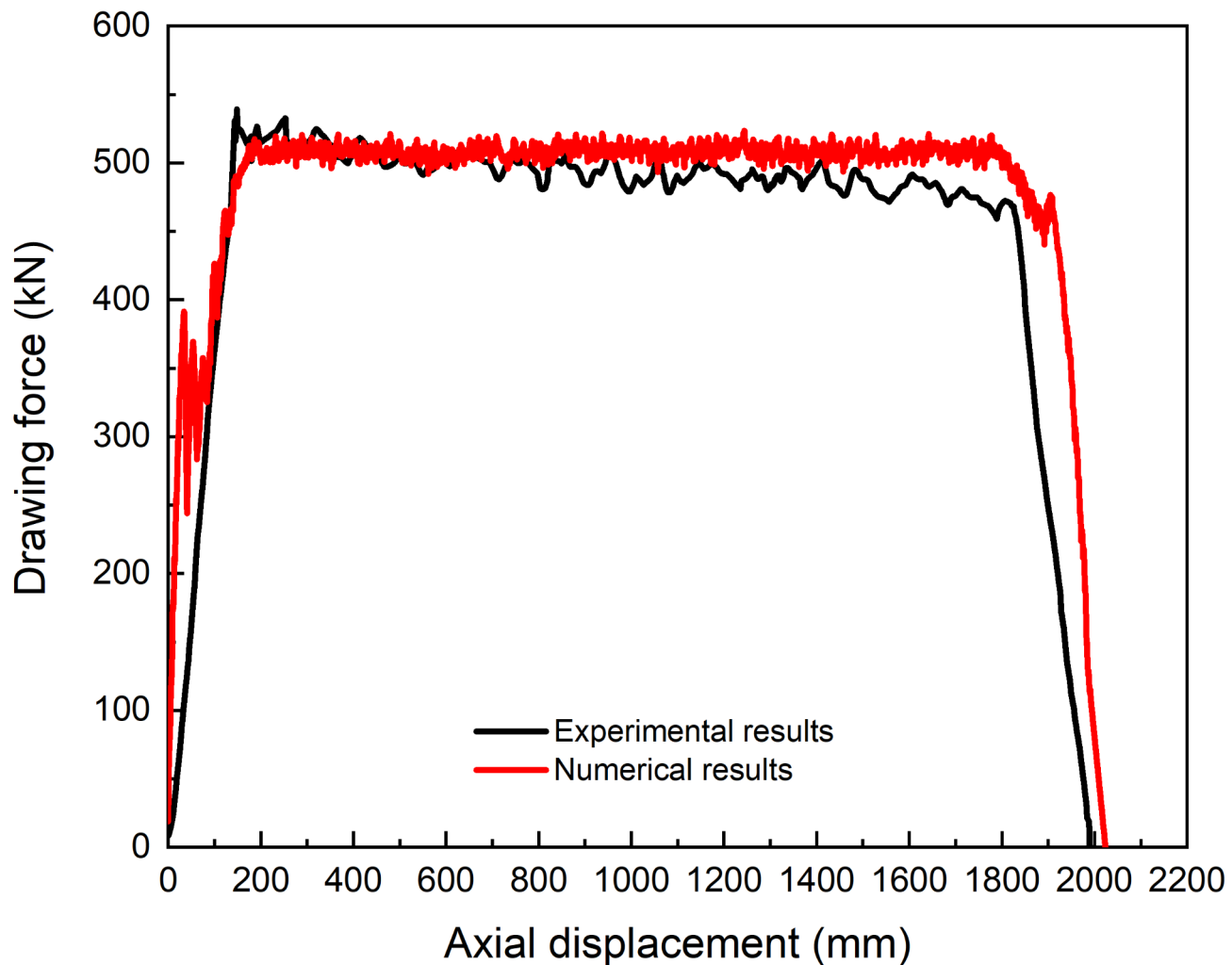


**Fig. 6.** Experimental and numerical drawing forces against axial displacement.

After calibrating based on the uniaxial compression tests, the numerical values of the modulus and strength for the sandstone and concrete coincide well with the experimental calculations. The enumeration of micro-parameters of parallel bonds in Table 4 is consistent with that of the macro-mechanical parameters in Table 3. Earlier research<sup>35</sup> has introduced the specific verification process.

#### Cementation on pipe-concrete interface

The pull-out strength of all cables/bolts is mainly determined by the bonding strength  $\tau_f$  and the bonding area  $2\pi rl$  and can be expressed using  $2\pi rl\tau_f$ . In the NPR cable reinforcement system, the surrounding sandstone is classified as hard rock in line with the specification of C30 concrete, and  $\tau_f$  can be considered 1300 kPa. For this bonding strength, two micro-parameters need calibration for the pipe-concrete interface due to the rock and anchorage agent simulated by DEM and FDM. In the DEM-FDM and FDM models for static pull-out tests, the sandstone and concrete have radial thicknesses of 14.5 mm and 76.25 mm respectively, with a length of 300 mm for both. The cable for pull-out tests was modeled using a cylinder with the same radius of 60.5 mm and a length of 500 mm to simulate the pipe-concrete interface of coupled FDM-DEM model in NPR cable reinforcement system. The axial velocities were restrained in the far end of the sandstone, and the radial movements were fixed on the outer circumferential surface in both pull-out models. Furthermore, a consistent velocity of 20 mm/min was imposed on the distal end of the cable. The residual strength closely approximates 9 kN, which aligns with the frictional angle of 150 as indicated in Table 6. The contact parameters on the pipe-concrete interface in DEM-FDM and FDM models are illustrated in Tables 5 and 6. In a prior study, detailed information regarding mechanical parameters and the calibration process for micro-mechanical parameters within the Discrete Element Method (DEM) has been provided<sup>35</sup>.

#### Numerical results and discussions about the NPR cable-rock interaction

Based on the validated mechanical parameters, the numerical dynamic pull-out tests of the NPR cable with surrounding rock were performed under drop heights of 0.2 m, 0.4 m and 0.6 m. For dynamic loads generated at 0.2 m and 0.6 m, the corresponding parameters were determined as:  $A_0 = 5.08 \times 10^6$  kPa,  $f = 100$  Hz

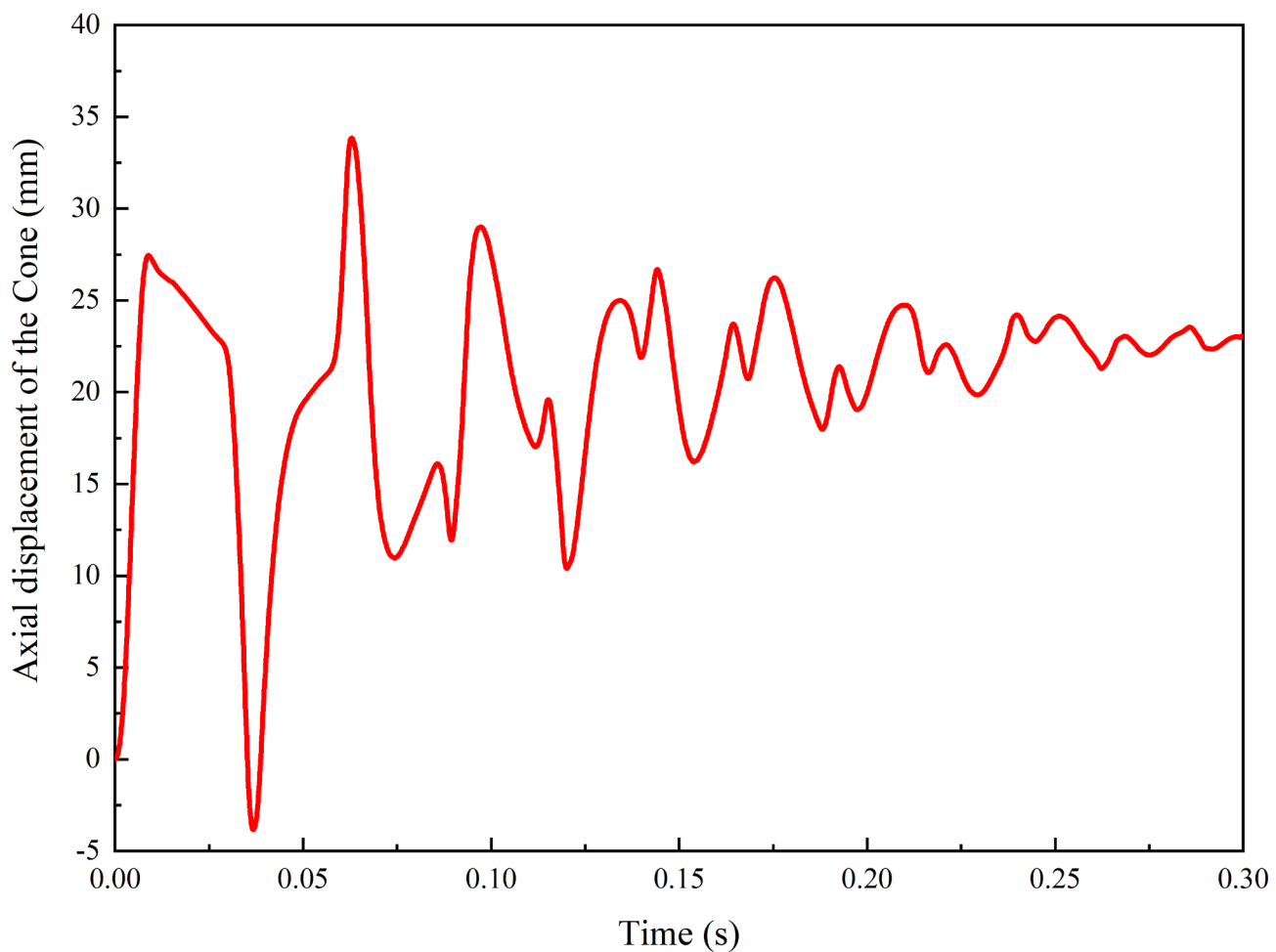


**Fig. 7.** The histories of impact force and axial displacement at the strand's end during the initial drop hammer impact.

(0.2 m) and  $A_0 = 9.14 \times 10^6$  kPa,  $f = 100$  Hz (0.6 m), respectively. The NPR cable-rock interaction, including the cone-pipe relative sliding displacement, the accumulated cone-pipe relative sliding displacement, the radial displacement of the pipe, the contact force of the concrete and rock, and the failure pattern of the concrete and surrounding sandstone, were investigated numerically in this section.

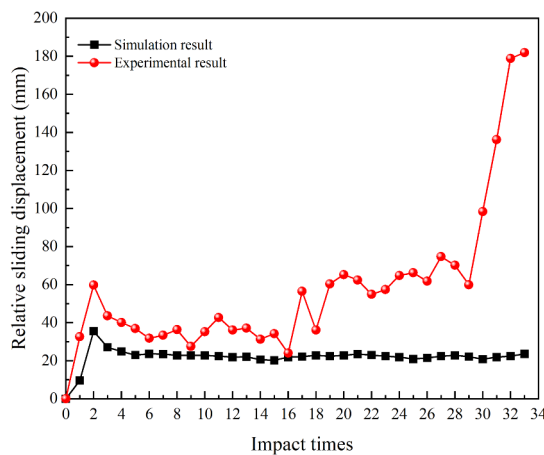
#### Relative sliding displacement of cone pipe

Different heights of the drop hammer represent varying impact loads, and the relative displacement between the cone and pipe also changes with the heights. For calculation cost, the DEM-FDM coupled model was subjected to 15 times dynamic loading with three drop hammer heights, as illustrated in Fig. 10a. After the 15th dynamic loading under different height conditions, the cumulative sliding distances of the cone are 202.9 mm, 343.2 mm and 440 mm, respectively. The relative sliding displacement between the cone and pipe under each impact load is significantly different due to the varying heights, as shown in Fig. 10b. It can be found that the relative displacement generated by the first three impact loads is relatively large since the front end of the cone is slimly smaller than the inner diameter of the pipe, and the cone does not fully contact the inner pipe wall. As the impact loading progresses, the cone is fully compressed and squeezed into the pipe. The relative sliding distances between the cone and pipe under 0.2 m, 0.4 m, and 0.6 m drop hammer heights remain constant, approximately 12 mm, 21 mm, and 31 mm, respectively.

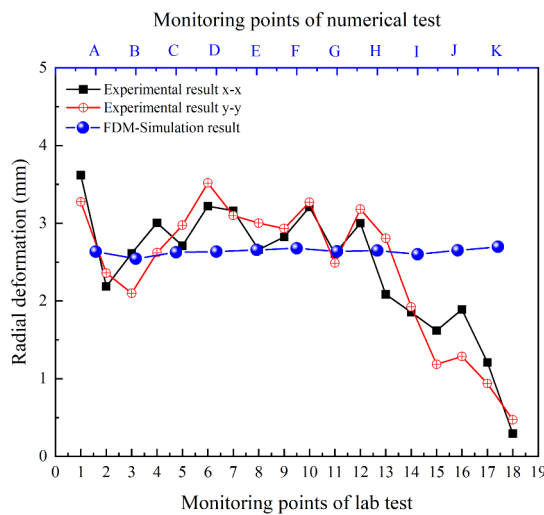
#### The radial displacement of the pipe

The radial displacement was obtained by setting 11 monitoring points (A–K) in Fig. 8c on the outer pipe wall under three drop heights. The average radial displacement of the outer surface corresponding to the drop heights of 0.2 m, 0.4 m, and 0.6 m is 2.2 mm, 2.4 mm, and 3.0 mm, respectively.

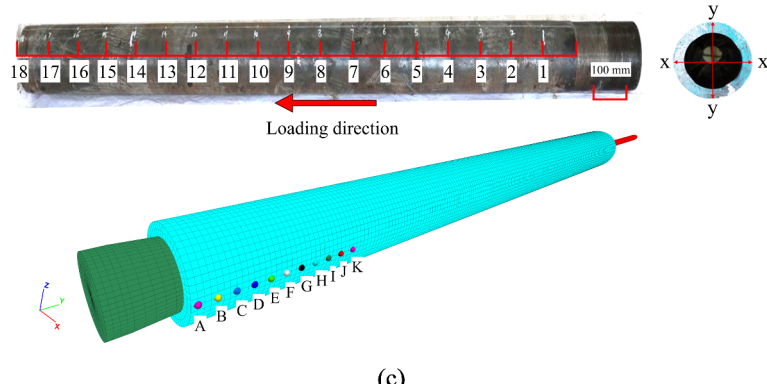
It can be seen from Fig. 10a that the cone's moving distances after 15 impacts with different drop heights are 198.9 mm, 341.2 mm, and 437 mm, respectively. It should be noted that the starting coordinate of the pipe is 72 mm, and the ending coordinate of the surrounding rock simulated by DEM is 372 mm. The cone was positioned in the middle of the pipe after the 15th impact load with a drop hammer height of 0.2 m, and the impact load exerted a minimal influence on the rear section of the pipe. The radial displacement after the F



(a)



(b)



(c)

**Fig. 8.** Comparison between simulation result and experimental results. (a) Relative cone-pipe sliding against impact time under drop hammer loadings; (b) radial displacement on the outer wall of pipe at different monitoring points; (c) monitoring points situation on the outside surface of pipe.

monitoring point is significantly reduced to 0. For the remaining two drop hammer heights, a consistent radial displacement was observed at each monitoring point located on the outer wall of the pipe as illustrated in Fig. 11.

#### Failure pattern of the concrete and surrounding sandstone

This subsection elucidates the micro-scale evidence to interpret the failure pattern and mechanism in the pipe's surrounding materials. We focus on the state of the end of the 8th dynamic impact under different drop hammer heights. Taking the front-end position of the impacted cone as a reference, the midpoints of four measurement volumes were selected at distances of 25 mm, 50 mm, and 110 mm. Each measured volume is a slice with a

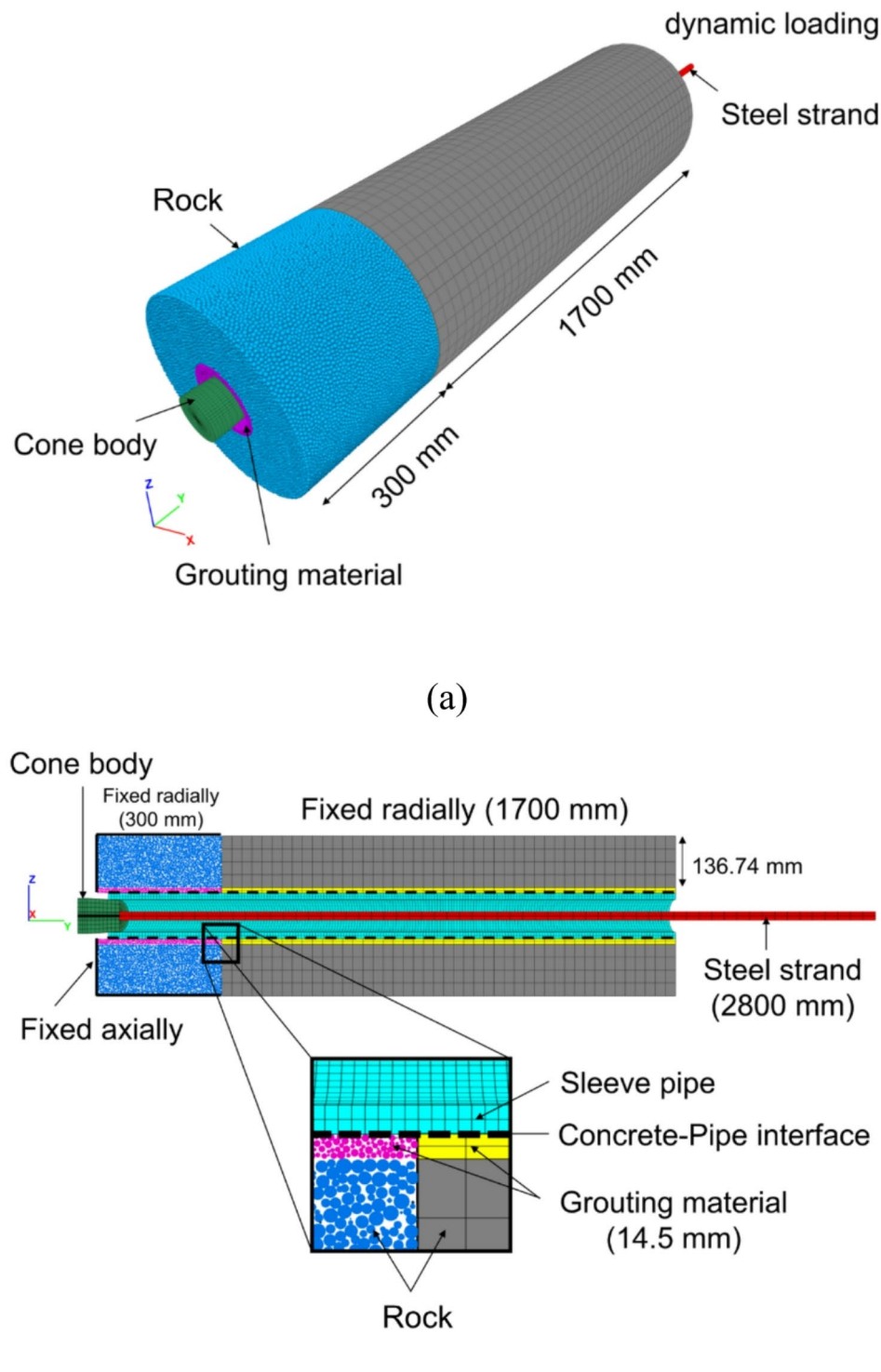


**Fig. 9.** Coupled DEM-FDM model of NPR cable reinforcement system. (a) The overview in 3D and (b) the profile in axial direction.

thickness of 1.5 times the  $D_{50}^{concrete}$ , where  $D_{50}^{concrete}$  represents the mean diameter of concrete particles, and it is oriented perpendicular to the y-axis.

The average contact stress  $\bar{\sigma}_n = \sum_c |\sigma_n^c| / N_c$  ( $\sigma_n^c$  represents the normal contact stress and  $N_c$  signifies the contact force) serves as a benchmark for evaluating the average normal stress within a sample volume. Regarding the height of three falling weights, the coordinates of the midpoint position of these measured volumes are:  $Y_1 = 102$  mm,  $Y_2 = 127$  mm,  $Y_3 = 157$  mm and  $Y_4 = 212$  mm (0.2 m);  $Y_1 = 181$  mm,  $Y_2 = 206$  mm,  $Y_3 = 236$  mm

	Young's modulus (GPa)	Poisson's ratio	Compression strength (MPa)	Cohesion (MPa)	Frictional angle (°)
Sandstone	29.4	0.25	147.0	20	40
Concrete	7.5	0.17	30.0	10	30

**Table 3.** Macro-mechanical parameters of sandstone and concrete C30.

Layers	Detachable linear set			Bonding set				
	Effective modulus $E^*$ (GPa)	Stiffness ratio $k_n/k_s$	Friction angle $\phi$ (°)	Effective modulus $\bar{E}^*$ (GPa)	Stiffness ratio $\bar{k}_n/\bar{k}_s$	Tension strength $\bar{\sigma}_c$ (MPa)	Cohesion $\bar{c}$ (MPa)	Friction angle $\bar{\phi}$ (°)
Sandstone	19.16	3.5	30	19.16	3.5	16.0	20.0	40
Concrete	4.98	3.7	15	4.98	3.7	3.0	10.0	30

**Table 4.** Micro-parameters of DEM contacts.

Detachable linear set			Bonding set				
Effective modulus $E^*$ (GPa)	Stiffness ratio $k_n/k_s$	Friction angle $\phi$ (°)	Effective modulus $\bar{E}^*$ (GPa)	Stiffness ratio $\bar{k}_n/\bar{k}_s$	Tension strength $\bar{\sigma}_c$ (MPa)	Cohesion $\bar{c}$ (MPa)	Friction angle $\bar{\phi}$ (°)
0.498	3.7	15	0.498	3.7	3.0	1.32	30

**Table 5.** Contact parameters on the interface between pipe and DEM concrete.

Stiffness-normal (GPa/m)	Stiffness-shear (GPa/m)	Tension strength (MPa)	Cohesion (MPa)	Friction angle $\bar{\phi}$ (°)	Cohesion (MPa)
8.5	3.7	1.92	1.92	15	0

**Table 6.** Contact parameters on the interface between pipe and FDM concrete.

and  $Y_4 = 291$  mm (0.4 m);  $Y_1 = 236$  mm,  $Y_2 = 261$  mm,  $Y_3 = 291$  mm and  $Y_4 = 346$  mm (0.6 m), respectively. Specifically,  $Y_1$  refers to the coordinates of the front end of the cone after the 8th dynamic impact.

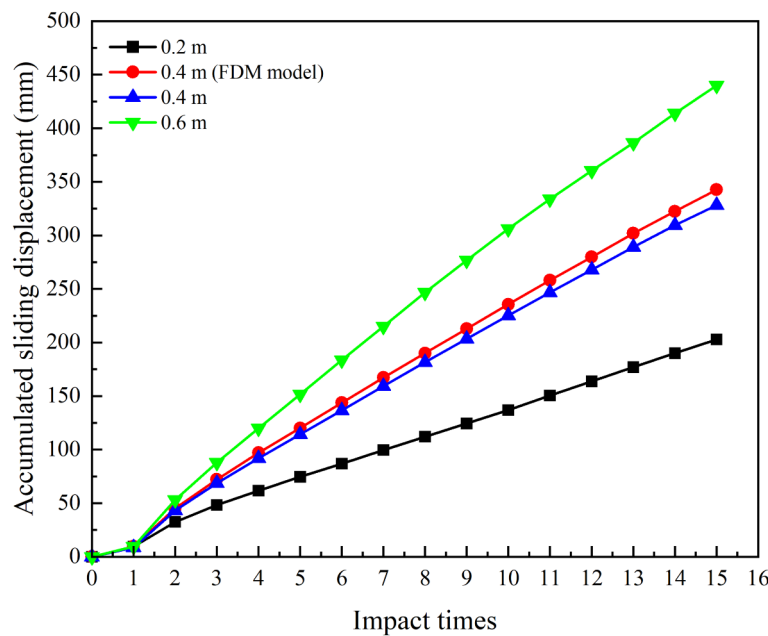
In Fig. 12, the force networks are presented, with red branches representing tensile stresses and black branches representing compressive stresses. The average thickness of the branches indicates the magnitude of the average normal stress  $\bar{\sigma}_n$ . In other words, a greater normal stress will produce thicker branches. The level of transparency in the visualization signifies the distance in the y-direction between the contact point and the midpoint of the respective measured volume. Regarding the evolution of the force networks, tensile stress is primarily distributed along the circumferential direction within the concrete and rock.

### Field application

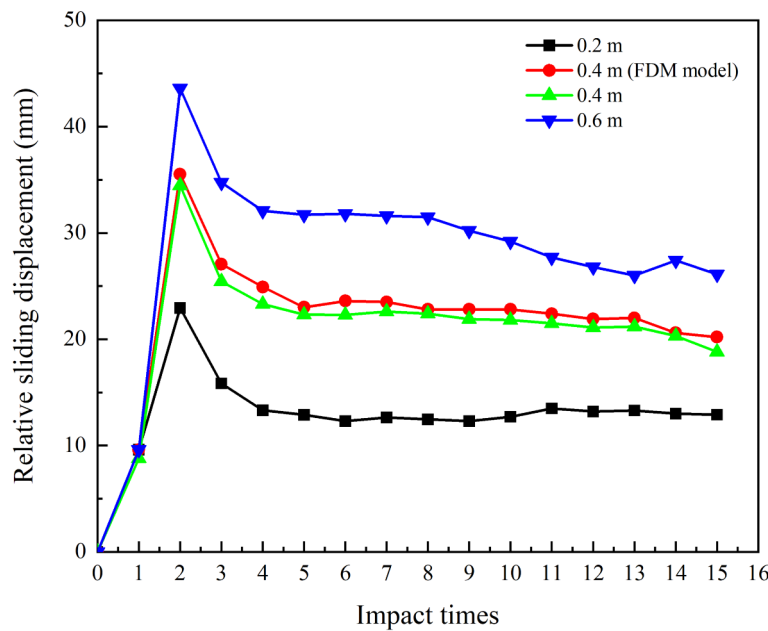
Nanfen opencast iron mine, situated in the Taizihe depression on the northern margin of Yingkou-Kuandian uplift within the Liaodong platform of the North China Platform, holds the distinction of being the largest single opencast iron mine in Asia. The orebody, embedded within the iron-bearing rock section of the Archean Anshan Group, exhibits a monoclinic structural formation. The footwall slope of the mining area belongs to a stone bedding slope, and nearly 60 landslides have occurred since 1964, forming an old landslide body with an area of about 110,000 m<sup>3</sup>, which seriously threatens the safe mining of the mine<sup>51</sup>.

The mining area has a bottom elevation of 160 m, while the elevation of the footwall slope near the pit wall is approximately 694 m, resulting in a high and steep slope with a height difference of about 534 m. The slope angle of this steep formation ranges from 46° to 54°. The rocks of the landslide body are mainly chlorite amphibole schist. Under natural moisture conditions, the uniaxial compressive strength is about 59.2 MPa, but under saturated conditions (continuous water absorption for 8 days), the uniaxial compressive strength drops to 22.71 MPa, demonstrating that water has a significant impact on the strength loss of this type of rock. During calibration efforts, it is crucial to accurately determine the geological and structural characteristics of this unique mining environment to ensure the reliability and safety of mining operations.

A landslide is a sliding phenomenon that occurs when the rock and soil mass of a slope slides along a continuous shear failure surface. Under the influence of landslide shear forces, conventional anchor bolts and cables, due to their limited extensibility, are highly prone to tensile failure. The aforementioned experimental studies and numerical analyses have demonstrated that NPR anchor cables possess exceptional mechanical properties that enable them to endure large deformations in rock masses under high constant resistance. Therefore, in open-pit mine slope engineering, by installing mechanical sensors with BeiDou satellite remote



(a)



(b)

**Fig. 10.** The cone-pipe sliding displacement: (a) the cone-pipe cumulative sliding displacement; (b) the cone-pipe relative sliding displacement.

communication capabilities at the free end of NPR anchor cables, NPR anchor cables have the potential to emerge as a comprehensive technology that integrates monitoring, early warning, and control into a single system.

To investigate the utilization of NPR cable in the integrated technology of monitoring, warning, and controlling slope stability in open pit mines, taking into account the structural characteristics and dimensions of the landslide body at the stope footwall of the Nanfen iron open pit, we have installed 30 NPR cable sliding force monitoring stations and 2 GPS surface displacement monitoring stations on the landslide. In Fig. 13, the dots

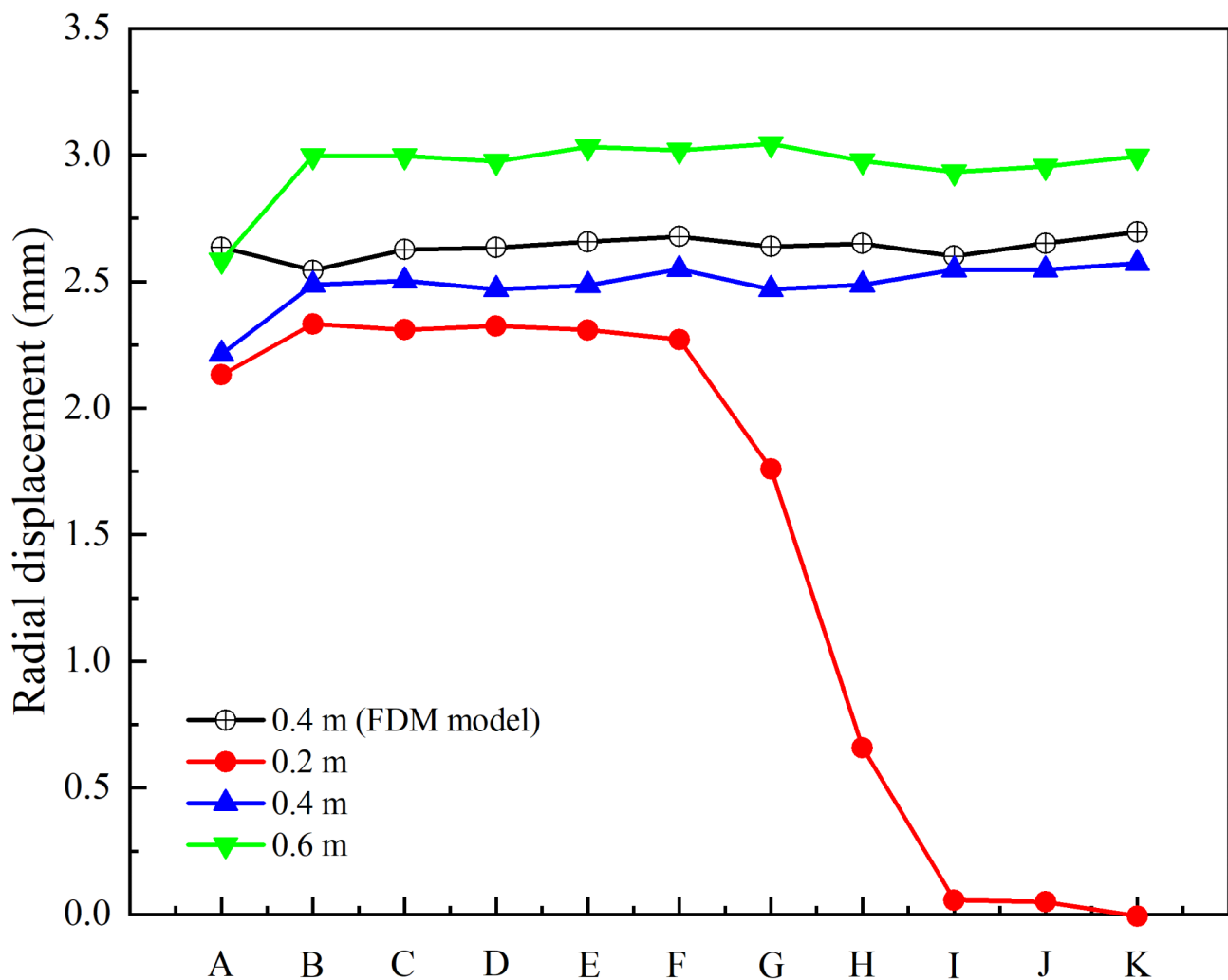


**Fig. 11.** The radial displacement on the outer wall of the pipe.

represent the deep sliding force monitoring points, while the yellow triangles indicate the initial GPS surface displacement monitoring points. Figure 14 depicts the cross-sectional features along the A–A' section line within the monitored area.

In early October 2011, the system provided an early warning for the impending “Rockslides 1005” near monitoring point No. 334-4, accurately predicting the event five days before it occurred. A qualitative analysis of the sliding force curve (depicted as the red curve) within the coupled monitoring data reveals that the NPR cable system is capable of offering advance notification throughout the entire progression of “Rockslides 1005”, as shown in Fig. 15. The detailed analysis is outlined below.

Prior to October 1, the monitoring sliding force curve within the No. 334-4 NPR coupling system exhibited minimal variations, remaining within acceptable error margins, indicating a level and relatively stable slope condition (blue stable signal). However, on October 1, the sliding force monitoring curve displayed a marked upward trend, despite no apparent cracks or slips detected on the ground surface. By October 2, the sliding force monitoring curve accelerated its upward trajectory, registering an increment of approximately 300 kN. A subsequent inspection revealed the emergence of numerous micro-fractures on the 322–334 m bench of the stop footwall. These fractures ranged in width from 15 to 40 cm and length from 1.5 to 5 m.

At 2:15 pm on October 3, the sliding force monitoring curve continued to rise rapidly. After a thorough site assessment, it was noted that on the 322 m bench where an excavator was operating. Micro-cracks on the 322–334 m bench slope extending from 3 to 9 m in length and 25 to 120 cm in width. Due to the sliding force increment reaching 400 kN, the monitoring system automatically triggered a yellow early warning signal (sub stability warning), based on the established warning criteria. Prompt action was taken to evacuate personnel and equipment from the hazardous area, halting mining operations to avert potential dangers. Later, at 14:20 pm on the same day, the coupling monitoring curve indicated that the sliding force increment had escalated to 800 kN, prompting the monitoring system to issue an orange warning (near sliding warning) in accordance with the warning criteria.

On October 4, the sliding force monitoring curve witnessed a continued yet relatively subdued rise, ultimately reaching an increment of 1000 kN. Promptly, the monitoring system activated a red warning, signaling an

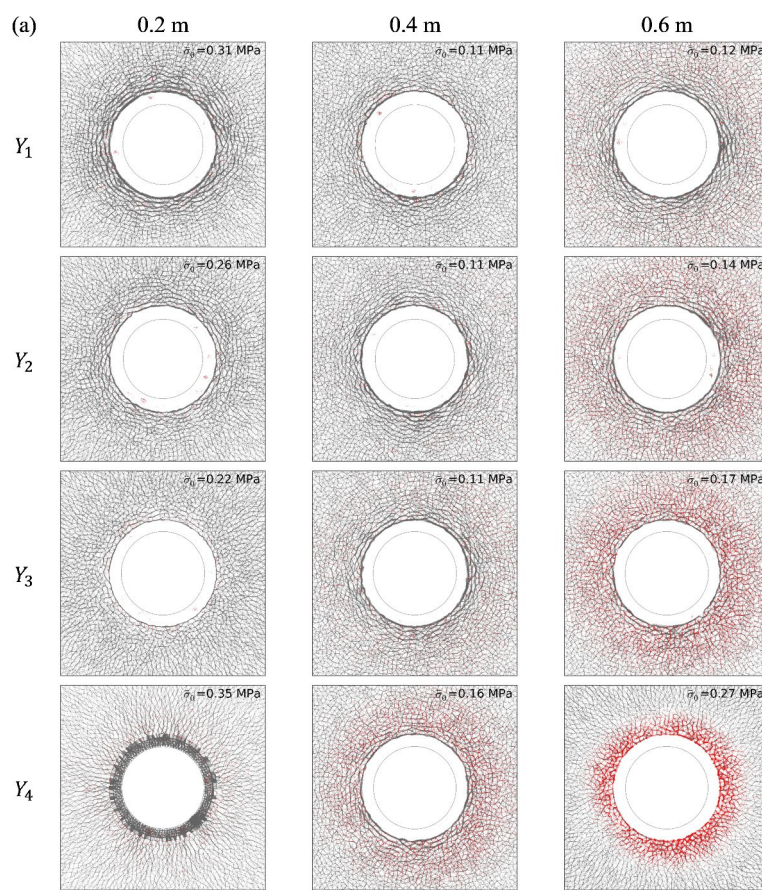


**Fig. 12.** Force network (depicted in terms of stress) in four measured volumes.

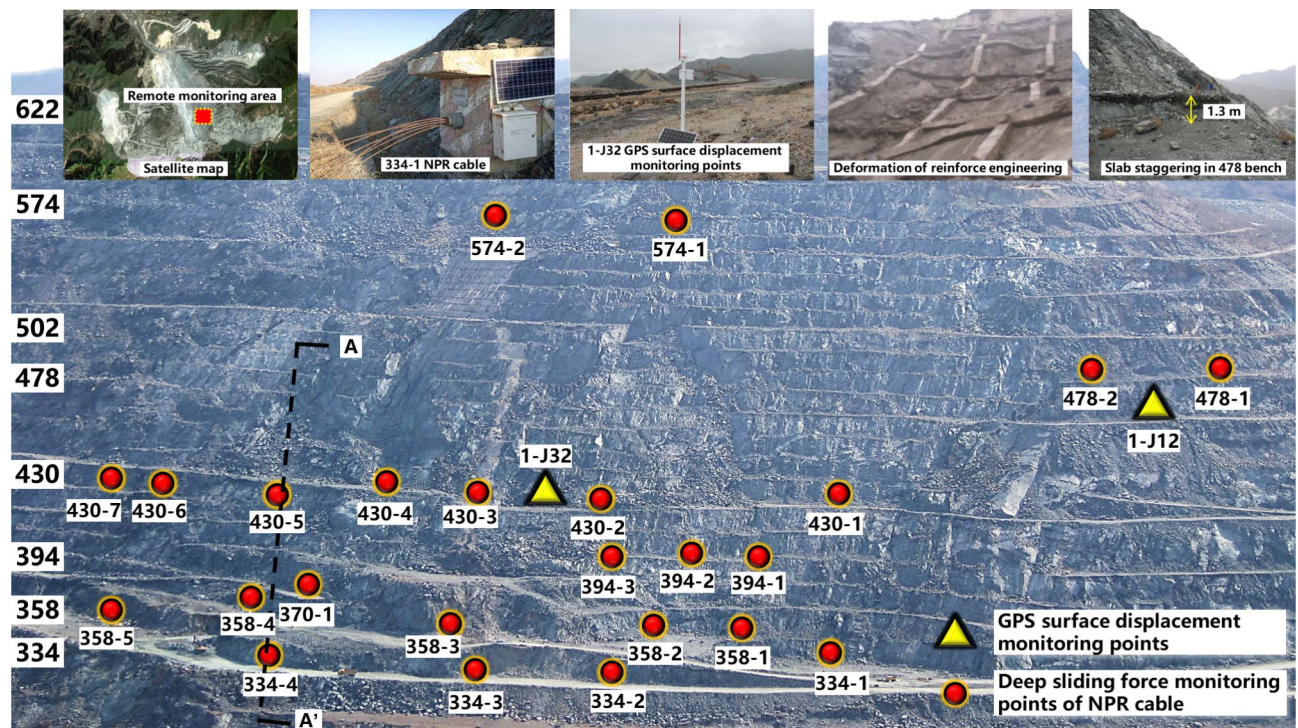


**Fig. 13.** Distribution characteristics of monitoring points.

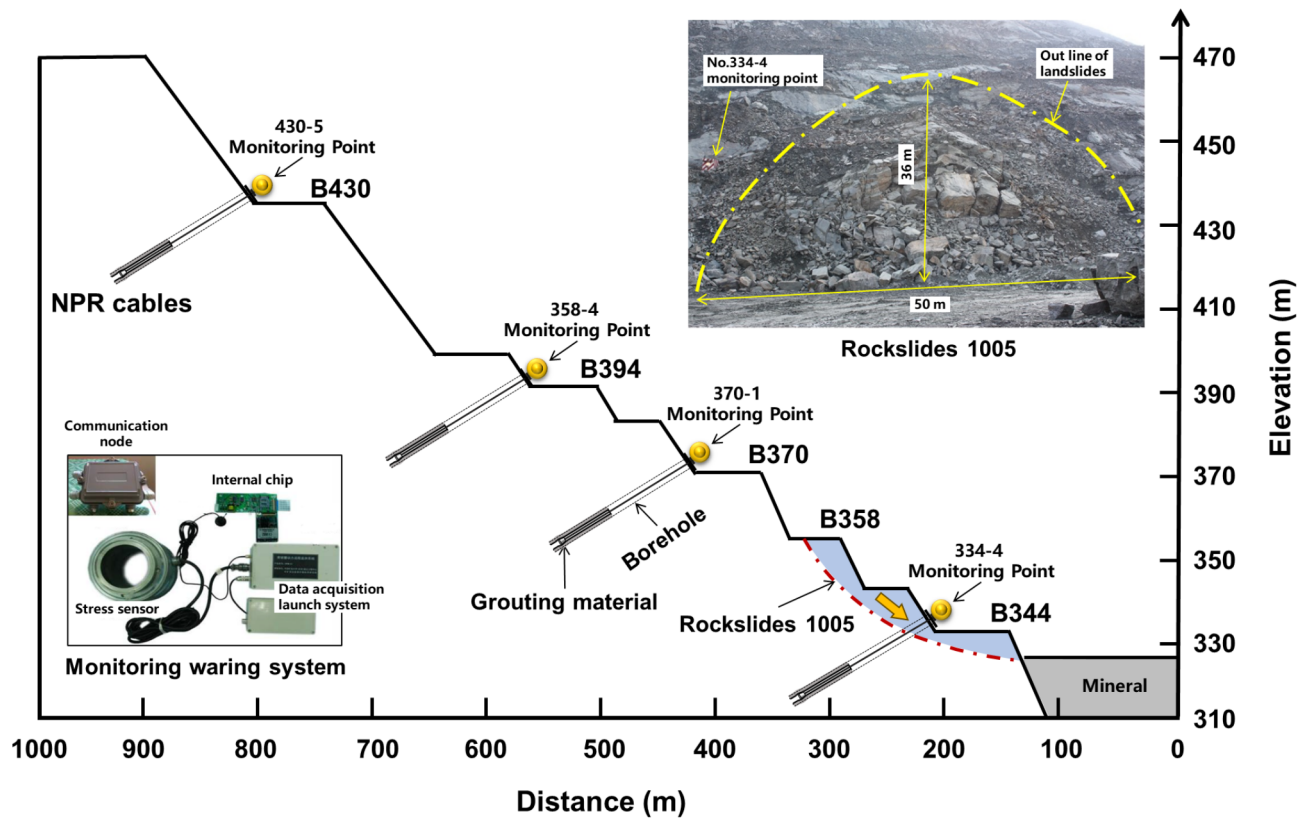


**Fig. 14.** Schematic diagram of A-A' cross section.

imminent sliding threat. Fortunately, swift evacuation of personnel and equipment prevented any casualties or property damage. The following day, at 19:00 on October 5, heavy rains lashed the Nanfen open-pit iron mine, accumulating approximately 31.8 mm of rainfall in just three hours. Shortly after, at 20:00, the sliding force curve in the coupling monitoring system underwent a sudden and significant drop, with the sliding force plunging from 1700 to 1400 kN. On October 6, at 9:00, we observed a landslide on the 322–358 m bench. The sliding mass exhibited a vertical height difference of approximately 36 m and a length spanning roughly 50 m from south to north. The characteristics of this landslide are depicted in Fig. 15.

The implementation of the NPR cable sliding force monitoring warning system for “Rocksides 1005” has resulted in a significant achievement: no casualties or property losses were incurred due to its timely alerts throughout the entire event.

## Conclusion

In this paper, the investigations describe the dynamic response of NPR cable under dynamic pull-out loading using experimental and numerical methods, reveal its interaction mechanism with rock, and can help predict and improve the performance of NPR cable in mitigating dynamic disasters, for example, the earthquake, explosion, and rock burst. The field application of the NPR cable sliding force monitoring warning system is carried out. The conclusions from this study are as follows.

- (1) An introduction to the components of the drop hammer impact test system and the NPR cable is provided. Through the impact test with 0.4 m drop hammer height, the cone-pipe relative sliding displacement, the impact load intensity, and the radial deformation on the outer surface of the cone pipe after each impact is obtained.
- (2) Dynamic pull-out test results under drop hammer impact loading and numerical outcomes of the DEM-FDM coupled NPR reinforcement system model are discussed and analyzed as follows: First, the evolution of cone-pipe relative sliding displacement and radial displacement distribution of pipe outer surface in drop hammer impact tests are evaluated. Second, the cone-pipe relative sliding displacement under three falling hammer heights (0.2, 0.4, and 0.6 m) is obtained. Third, the penetration of cone body negatively impacts the contact with the front rock. Fourth, we delved into the failure mode and radial displacement field of the concrete and the surrounding sandstone microscopically.
- (3) The landslide monitoring results from the Nanfen iron open pit demonstrate that the NPR cable's exceptional mechanical properties, such as its capacity for significant deformation, high constant resistance, and resilience to tensile failure, were thoroughly validated. Additionally, this exercise underscores the tremen-

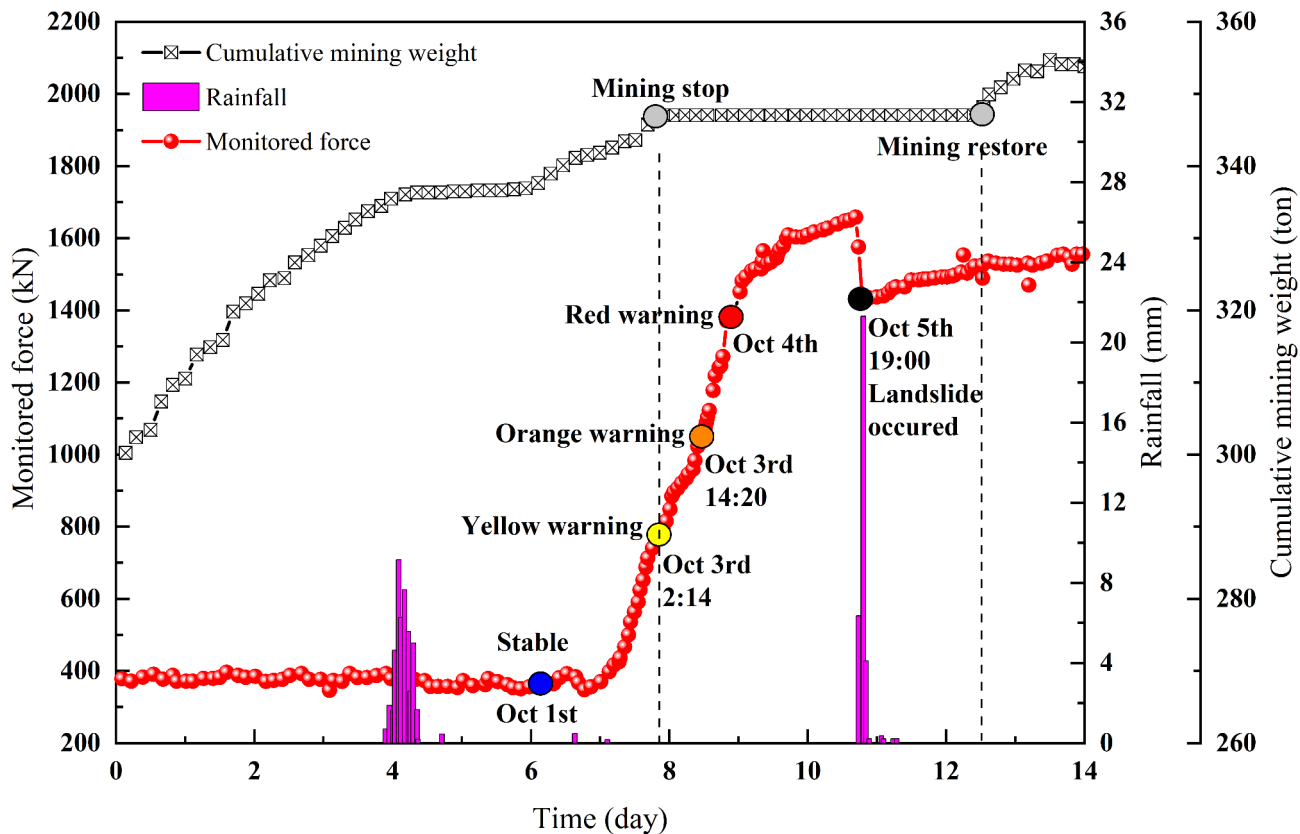


**Fig. 15.** Monitored force and rainfall coupling monitoring curve of No. 334-4 monitoring point.

dous potential of NPR cable in enhancing, preventing, monitoring, and providing early warnings for slope failures in open pit mines.

### Data availability

Data will be made available on request. Please contact the corresponding author.

Received: 14 May 2024; Accepted: 11 February 2025

Published online: 10 May 2025

### References

1. Jin-feng, Z. & Peng-hao, Z. Analytical model of fully grouted bolts in pull-out tests and in situ rock masses. *Int. J. Rock Mech. Min. Sci.* **113**, 278–294 (2019).
2. Hu, J. et al. Rockburst hazard control using the excavation compensation method (ECM): A case study in the Qinling Water Conveyance tunnel. *Engineering* **34**, 154–163. <https://doi.org/10.1016/j.eng.2023.11.013> (2024).
3. Tao, Z. et al. Mechanical evolution of constant resistance and large deformation anchor cables and their application in landslide monitoring. *Bull. Eng. Geol. Environ.* **78** (7), 4787–4803 (2019).
4. Li, H. R. et al. Effect of water on mechanical behavior and acoustic emission response of sandstone during loading process: Phenomenon and mechanism. *Eng. Geol.* **294**, 106386. <https://doi.org/10.1016/j.enggeo.2021.106386> (2021).
5. Li, H. R. et al. Effect of water saturation on dynamic behavior of sandstone after wetting-drying cycles. *Eng. Geol.* **319**, 107105. <https://doi.org/10.1016/j.enggeo.2023.107105> (2023).
6. Li, C. C. A new energy-absorbing bolt for rock support in high stress rock masses. *Int. J. Rock Mech. Min. Sci.* **47**(3), 396–404 (2010).
7. St-Pierre, L., Hassani, F., Radziszewski, P. & Ouellet, J. Development of a dynamic model for a cone bolt. *Int. J. Rock Mech. Min. Sci.* **46** (1), 107–114 (2009).
8. Charette, F. & Plouffe, M. A new rock bolt concept for underground excavations under high stress conditions. In *Proceedings of 6th International Symposium on Ground Support in Mining and Civil Engineering Construction*, Johannesburg 225–240 (2008).
9. Ozbay, U. & Neugebauer, E. In-situ pull testing of a yieldable rock bolt, ROOFEX. *Control. Seismic Hazard. Sustain. Dev. Deep Mines* **2**, 1081–1090 (2009).
10. Li, C. C. Field observations of rock bolts in high stress rock masses. *Rock Mech. Rock Eng.* **43**(4), 491–496 (2010).
11. Zhao, X. et al. Dynamic and static analysis of a kind of novel J energy-releasing bolts. *Geomat. Nat. Hazards Risk* **11**(1), 2486–2508 (2020).
12. He, M. et al. Development of a novel energy-absorbing bolt with extraordinarily large elongation and constant resistance. *Int. J. Rock Mech. Min. Sci.* **67**, 29–42 (2014).
13. He, M. & Guo, Z. Mechanical property and engineering application of anchor bolt with constant resistance and large deformation. *Chin. J. Rock Mech. Eng.* **33**(7), 1297–1308 (2014).
14. He, M., Li, C. & Gong, W. Elongation and impacting experimental system for bolts with constant resistance and large deformation and finite element analysis. *Chin. J. Rock. Mech. Eng.* **34**(11), 2161–2178 (2015).

15. Zhi-gang, T., Hai-peng, L., Guang-lin, S., Li-jie, Y. & Xiu-lian, Z. Development of monitoring and early warning system for landslides based on constant resistance and large deformation anchor cable and its application. *Rock Soil Mech.* **36**(10), 3032–3040 (2015).
16. He, M., Li, C., Gong, W., Sousa, L. & Li, S. Dynamic tests for a constant-resistance-large-deformation bolt using a modified SHTB system. *Tunn. Undergr. Space Technol.* **64**, 103–116 (2017).
17. Sun, X. et al. Mechanical properties and supporting effect of CRLD bolts under static pull test conditions. *Int. J. Miner. Metall. Mater.* **24**, 1–9 (2017).
18. Hu, J., Li, Z. & Feng, J. Analytical model of elasto-plastic and numeric analysis for the constant resistance large deformation (NPR) cable. *Chin. J. Rock Mech. Eng.* **38**(S2), 3565–3574 (2019).
19. Khaleghparast, S., Aziz, N., Remennikov, A. & Anzaniour, S. An experimental study on shear behaviour of fully grouted rock bolt under static and dynamic loading conditions. *Tunn. Undergr. Space Technol.* **132**, 104915 (2023).
20. Tao, Z. et al. Negative Poisson's ratio and peripheral strain of an NPR anchor cable. *J. Mt. Sci.* **19**(8), 2435–2448 (2022).
21. Ansell, A. Laboratory testing of a new type of energy absorbing rock bolt. *Tunn. Undergr. Space Technol.* **20**(4), 291–300 (2005).
22. Tao, Z., Pang, S., Zhou, Y., Zhang, H. & Peng, Y. Static pull testing of a new type of large deformation cable with constant resistance. *Adv. Mater. Sci. Eng.* **2017**, 5198049 (2017).
23. Wang, Q. et al. Dynamic mechanical characteristics and application of constant resistance energy-absorbing supporting material. *Int. J. Min. Sci. Technol.* **32**(3), 447–458 (2022).
24. Aziz, N. et al. An experimental study on the Shear performance of fully encapsulated Cable bolts in single shear test. *Rock Mech. Rock Eng.* **51**(7), 2207–2221 (2018).
25. Mirzaghorbanali, A. et al. Shear strength properties of cable bolts using a new double shear instrument, experimental study, and numerical simulation. *Tunn. Undergr. Space Technol.* **70**, 240–253 (2017).
26. Li, L., Hagan, P. C., Saydam, S., Hebblewhite, B. & Zhang, C. A laboratory study of shear behaviour of rockbolts under dynamic loading based on the drop test using a double shear system. *Rock Mech. Rock Eng.* **52**(9), 3413–3429 (2019).
27. Hu, J. et al. Control effect of negative Poisson's ratio (NPR) cable on impact-induced rockburst with different strain rates: An experimental investigation. *Rock Mech. Rock Eng.* **56**, 5167–5180 (2023).
28. Yi, X. & Kaiser, P. K. Impact testing for rockbolt design in rockburst conditions. *Int. J. Rock. Mech. Min. Sci. Geomech. Abstracts* **31**(6), 671–684 (1994).
29. St-Pierre, L., Hassani, F. P., Radziszewski, P. H. & Ouellet, J. Development of a dynamic model for a cone bolt. *Int. J. Rock Mech. Min. Sci.* **46**(1), 107–114 (2009).
30. He, M. et al. Dynamic properties of micro-NPR material and its controlling effect on surrounding rock mass with impact disturbances. *Undergr. Space* **15**, 331–352 (2024).
31. He, M., Tao, Z. & Zhang, B. Application of remote monitoring technology in landslides in the Luoshan mining area. *Min. Sci. Technol.* **19**(5), 609–614 (2009).
32. Li, Z. et al. Laboratory testing and modeling of a high-displacement cable bolt. *Int. J. Geomech.* **19**(7), 04019078 (2019).
33. Hu, J., Li, Z., Darve, F. & Feng, J. Advantages of second-order work as a rational safety factor and stability analysis of a reinforced rock slope. *Can. Geotech. J.* **57**(5), 661–672 (2020).
34. He, M. & Sousa, L. Experiments on rock burst and its control. In *Australasian Ground Control in Mining Conference*, Sidney 19–31 (2014).
35. Li, Z., Hu, J., Zhu, H., Feng, J. & He, M. Numerical study on the CRLD cable–rock interaction under static pull-out loading using coupled DEM–FDM method. *Acta Geotech.* **15**, 2137–2158 (2020).
36. Munjiza, A. et al. Structural applications of the combined finite–discrete element method. *Comput. Part. Mech.* **7**(5), 1029–1046 (2020).
37. Song, W. & Hong, R. PFC/FLAC coupled numerical simulation of excavation damage zone in deep schist tunnel. *Appl. Mech. Mater.* **236**, 622–626 (2012).
38. Shi, H., Zhang, H., Chen, W., Song, L. & Li, M. Pull-out debonding characteristics of rockbolt with prefabricated cracks in rock: A numerical study based on particle flow code. *Comput. Part. Mech.* **11**, 29–53 (2023).
39. Dong, Z. H. et al. Coupled FEM/DEM modeling for the pull-out failure of corroded rockbolt. *Comput. Part. Mech.* **11**, 1599–1611 (2023).
40. He, M., Guo, A., Meng, Z., Pan, Y. & Tao, Z. Impact and explosion resistance of NPR Anchor cable: Field test and numerical simulation. *Undergr. Space* **10**, 76–90 (2023).
41. Martin, L. B., Tijani, M., Hadj-Hassen, F. & Noiret, A. Assessment of the bolt–grout interface behaviour of fully grouted rockbolts from laboratory experiments under axial loads. *Int. J. Rock Mech. Min. Sci.* **63**, 50–61 (2013).
42. Nemcik, J., Ma, S., Aziz, N., Ren, T. & Geng, X. Numerical modelling of failure propagation in fully grouted rock bolts subjected to tensile load. *Int. J. Rock Mech. Min. Sci.* **71**, 293–300 (2014).
43. Wang, S. et al. Numerical investigation of coal pillar failure under simultaneous static and dynamic loading. *Int. J. Rock Mech. Min. Sci.* **84**, 59–68 (2016).
44. Wang, H., Jiang, Y., Zhao, Y., Zhu, J. & Liu, S. Numerical Investigation of the dynamic mechanical state of a coal pillar during longwall mining panel extraction. *Rock Mech. Rock Eng.* **46**(5), 1211–1221 (2013).
45. Cundall, P. A. & Strack, O. D. A discrete numerical model for granular assemblies. *Geotechnique* **29**(1), 47–65 (1979).
46. Potyondy, D. O. & Cundall, P. A bonded-particle model for rock. *Int. J. Rock Mech. Min. Sci.* **41**(8), 1329–1364 (2004).
47. Cai, M. et al. FLAC/PFC coupled numerical simulation of AE in large-scale underground excavations. *Int. J. Rock Mech. Min. Sci.* **44**(4), 550–564 (2007).
48. Li, Y., Han, X., Ji, J. & Wang, H. Research of rigid-pile composite foundation with crushed stone cushion based on FDM–PFC coupling method. *Geomechanics from Micro to Macro – Soga et al. (Eds)© 2015 Taylor & Francis Group, London, ISBN 978-1-138-02707-7.*
49. Moosavi, M. & Grayeli, R. A model for cable bolt–rock mass interaction: Integration with discontinuous deformation analysis (DDA) algorithm. *Int. J. Rock Mech. Min. Sci.* **43**(4), 661–670 (2006).
50. Jiang, Y., Wu, X., Wang, G., Li, B. & Iura, T. Interaction mechanism of yielding rock bolt and matrix mass. *ISRM Congress, ISRM-13CONGRESS-2015-201* (2015).
51. Tao, Z., Zhang, H., Chen, Y. & Jiang, C. Support principles of NPR bolt/cable and control techniques of large-deformation disasters. *Int. J. Min. Sci. Technol.* **26**(6), 967–973 (2016).

## Acknowledgements

This work was supported by Collaborative Innovation Center for Prevention and Control of Mountain Geological Hazards of Zhejiang Province (PCMGRH-2022-03), and the Foundation of State Key Laboratory for Geomechanics and Deep Underground Engineering, China University of Mining & Technology, Beijing (Grant No. SKLGDUEK 2217).

## Author contributions

Dr. J.H.: Investigation, writing and data curation and funding acquisition; Prof. M.H.: supervision, resources;

Prof. Z.T.: Investigation, writing—review & editing; Mr. H.Z.: Methodology, review and revision and funding acquisition.

## Declarations

### Competing interests

The authors declare no competing interests.

### Additional information

**Correspondence** and requests for materials should be addressed to H.Z.

**Reprints and permissions information** is available at [www.nature.com/reprints](http://www.nature.com/reprints).

**Publisher's note** Springer Nature remains neutral with regard to jurisdictional claims in published maps and institutional affiliations.

**Open Access** This article is licensed under a Creative Commons Attribution-NonCommercial-NoDerivatives 4.0 International License, which permits any non-commercial use, sharing, distribution and reproduction in any medium or format, as long as you give appropriate credit to the original author(s) and the source, provide a link to the Creative Commons licence, and indicate if you modified the licensed material. You do not have permission under this licence to share adapted material derived from this article or parts of it. The images or other third party material in this article are included in the article's Creative Commons licence, unless indicated otherwise in a credit line to the material. If material is not included in the article's Creative Commons licence and your intended use is not permitted by statutory regulation or exceeds the permitted use, you will need to obtain permission directly from the copyright holder. To view a copy of this licence, visit <http://creativecommons.org/licenses/by-nc-nd/4.0/>.

© The Author(s) 2025